



HAL
open science

Second-Life Batteries Modeling for Performance Tracking in a Mobile Charging Station

Marwan Hassini, Eduardo Redondo-Iglesias, Pascal Venet

► **To cite this version:**

Marwan Hassini, Eduardo Redondo-Iglesias, Pascal Venet. Second-Life Batteries Modeling for Performance Tracking in a Mobile Charging Station. World Electric Vehicle Journal, 2023, 14 (4), pp.94. 10.3390/wevj14040094 . hal-04058691

HAL Id: hal-04058691

<https://hal.science/hal-04058691>

Submitted on 5 Apr 2023

HAL is a multi-disciplinary open access archive for the deposit and dissemination of scientific research documents, whether they are published or not. The documents may come from teaching and research institutions in France or abroad, or from public or private research centers.

L'archive ouverte pluridisciplinaire **HAL**, est destinée au dépôt et à la diffusion de documents scientifiques de niveau recherche, publiés ou non, émanant des établissements d'enseignement et de recherche français ou étrangers, des laboratoires publics ou privés.



Article

Second-Life Batteries Modeling for Performance Tracking in a Mobile Charging Station

Marwan Hassini ^{1,2,3,*} , Eduardo Redondo-Iglesias ^{1,3} and Pascal Venet ^{2,3}

¹ LICIT-ECO7 Lab, Univ Eiffel, ENTPE, Univ Lyon, 69500 Bron, France

² Univ Lyon, Université Claude Bernard Lyon 1, INSA Lyon, Ecole Centrale de Lyon, CNRS, Ampère, UMR5005, 69622 Villeurbanne, France

³ Eco7/Ampère Joint Research Team for Energy Management and Storage for Transport, 69500 Bron, France

* Correspondence: marwan.hassini@univ-eiffel.fr

Abstract: Lithium-ion batteries are seen as a key element in reducing global greenhouse gas emissions from the transport and energy sectors. However, efforts are still needed to minimize their environmental impact. This article presents a path towards a circular economy and more sustainable batteries, thanks to their reuse in mobile charging stations for electric vehicles. This work presents the results of characterization tests and modeling of second life batteries. The presented characterization test and electrical models can be used as references to evaluate the performance of aged batteries after their first life. Detailed test procedures and data results are provided in an open-access data paper.

Keywords: second life battery; reuse; charging; sustainability; modeling; equivalent circuit model; open science



Citation: Hassini, M.;

Redondo-Iglesias, E.; Venet, P.

Second-Life Batteries Modeling for Performance Tracking in a Mobile Charging Station. *World Electr. Veh. J.* **2023**, *14*, 94. <https://doi.org/10.3390/wevj14040094>

Academic Editor: Joeri Van Mierlo

Received: 27 February 2023

Revised: 24 March 2023

Accepted: 28 March 2023

Published: 3 April 2023



Copyright: © 2023 by the authors. Licensee MDPI, Basel, Switzerland. This article is an open access article distributed under the terms and conditions of the Creative Commons Attribution (CC BY) license (<https://creativecommons.org/licenses/by/4.0/>).

1. Introduction

Mitigating climate change is seen as a major challenge for the 21st century. According to the latest report from the Intergovernmental Panel on Climate Change, transport and electricity generation are responsible for 18% and 36% of the global greenhouse gas emissions, respectively [1]. To reduce this pollution, electrified vehicles and renewable energies are presented as interesting options. For these applications, lithium-ion batteries are key energy storage elements [1,2].

In 2021, 340 GWh of batteries have been produced, and these quantities are expected to increase significantly, possibly reaching 3500 GWh per year by 2030 [3]. In other words, to date, 10.8 kWh of batteries are currently being produced every second. Unfortunately, it is well known that their production is not yet sustainable. This means that none of the lithium-ion batteries produced can be manufactured without using natural resources and significant amounts of energy. Larcher and Tarascon pointed out that it takes over 400 kWh of energy to produce 1 kWh of lithium-ion battery with over 75% of this energy consumed during the material production phase [4]. In order to achieve sustainable energy production and transport, it is essential to develop solutions to reduce the negative impact of both the batteries already on the market as well as on the future generations of batteries.

The waste management hierarchy shown in Figure 1 establishes an order of preference for actions to reduce and manage waste [5]. Reduction, reuse, recycling, recovery and disposal are the actions that should be taken to reduce the environmental impact of a product. Reduction is the preferred action and consists of designing the product in order to limit the waste it will generate at the end of its life. In the context of batteries, reduction consists of minimizing the number of materials used in a battery, in other words, reducing the size of the battery. Electric vehicles powered by smaller batteries would be more economical and more environmentally-friendly [6,7].

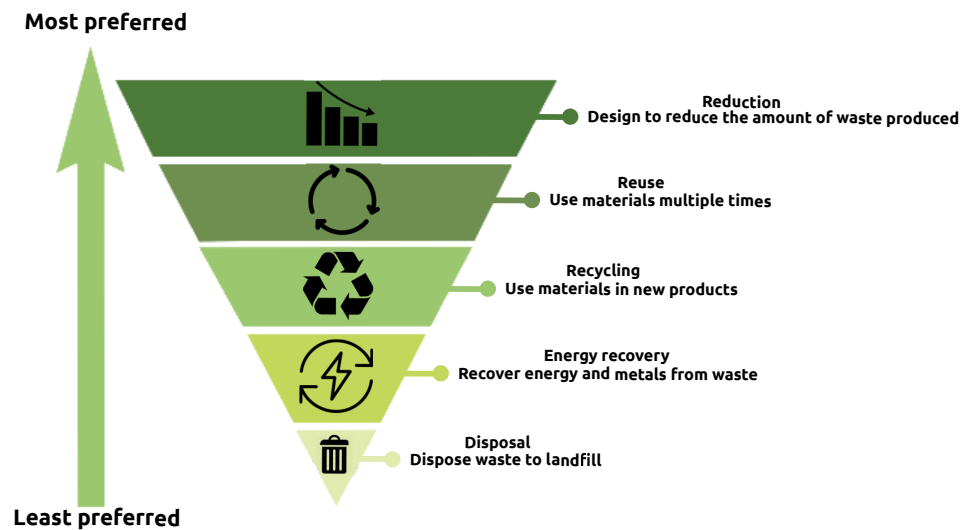


Figure 1. Waste Management Hierarchy.

However, such vehicles would have a shorter range and would be more dependent on charging infrastructure. To enable this shift, a reliable charging network needs to be developed. Mobile chargers are a solution to strengthen the existing infrastructure system. A mobile charging station can be defined as a charger capable of delivering energy to vehicles autonomously, i.e., without human assistance and without the need for an external power supply. This technology has the advantage of maximizing the utilization rate of the charging station as these chargers are able to move from one vehicle to another. They also provide a more flexible charging solution, as they are designed to be quickly deployed at any location, with the ability to adapt the energy embedded and the duration of stay to the needs of the drivers [8,9]. Figure 2 shows two autonomous mobile charging stations.



Figure 2. Mobile charging stations from Mob-Energy [10] and Volkswagen [11].

As the energy stored by these robot-like chargers is limited, they should be considered as a complementary technology to fixed chargers. To date, existing mobile charging stations can deliver up to 30 kWh at a maximum charging rate of 50 kW [12]. Powering these mobile charging stations with reused batteries is possible and would be a further step towards a circular economy. Reuse can be defined as the complete or partial reuse of the battery for the original purpose for which it was designed [13]. In the literature, reused batteries are commonly referred to as “second life batteries”.

While there is a broad consensus in the battery community to recognize the environmental benefits of reuse, the economic interest of second life batteries is still being debated. Finding applications that could accept the constraints of reused batteries is still a challenge. To date, most studies have focused on stationary applications [14–17]. Since the volume required for these applications is limited, few authors have presented mobile applications as an interesting alternative [18–20]. In addition to the application choice, battery performance evolution needs to be carefully tracked as it has a significant impact on the economic interest of battery reuse [21,22].

Although research about second life batteries is gaining interest, two important limitations of the existing studies remain:

First, two definitions of battery reuse coexist in the literature. Most authors define second life batteries in terms of performance level. A threshold of 20 or 30% capacity loss is often considered as the boundary between first and second life [23–26]. Studies considering this definition answer the following research question: how does the performance of deeply aged batteries evolve? Other authors define reused batteries as batteries that have undergone a change of application [27,28]. This definition raises another research question: what is the effect of an application change on the evolution of battery performance? To date, there is a lack of experimental or modeling studies investigating the performance evolution of a battery that has undergone an application change. This is an important gap since the operating conditions can vary significantly from the first life to the second life.

Secondly, much of the existing research has examined batteries that have been aged in a laboratory. This method has been preferred because of the complexity of acquiring batteries after their electric vehicle life. Laboratory studies also allow control of operating conditions during the whole life of the battery. Nevertheless, in real-world situations users of second life batteries do not have access to the data during first-life use. The battery performance must be assessed to determine the battery's suitability for a second life. In recent years, few studies have assessed the performance of batteries extracted from electric vehicles [29–31]. Nevertheless, these papers are pioneer works focusing on experimental performance assessment. No work has yet been carried out on the electrical modeling of such batteries. Further studies should be conducted to get more insights into battery reuse after the automotive life.

1.1. Contributions

The authors aim to fill the gaps described above by presenting an experimental and modeling study on a battery extracted from an electric vehicle and reused in a mobile application. This article contributes to the existing research on second life batteries in various aspects.

1. Description of a new possible application for second life batteries

In this article, a new possible application for second life batteries is presented: the mobile charging station. To the best of the authors' knowledge, this is one of the first studies to present in detail a mobile application for reused batteries.

2. Experimental evaluation of second life battery performance

In this study, a characterization test is performed to evaluate the performance and calibrate the electrical models of the second life battery. The capacity of the battery cell is measured at three temperatures and the resistance of the battery cell is characterized at the same three temperatures using current at various charge/discharge rates and depths of discharge. This experimental work contributes to the existing literature on second life batteries as it is one of the first to evaluate the performance of a high-capacity prismatic cell extracted from real second life electric vehicle battery modules.

3. Modeling second life battery performance

This study presents two electrical models that can be used as a reference to evaluate and emulate second life battery performance. The influence of usage profile and temperature on model accuracy is also evaluated. This modeling work is central to estimating the energy stored in the mobile charging station, which is the first step in developing pricing, charging schedules, and energy management strategies. This is one of the first articles to model a second life battery cell extracted from an electric vehicle.

4. Open access publishing of the experimental data and software

Experimental data recorded during the characterization test are published as open-source along with the article. The open software used for data processing has also been shared. To the best of the authors' knowledge, this is one of the first articles to share experimental data on second life batteries and the software used to analyze these data [32–34].

1.2. Layout

The article is organized as follows: Section 2 presents the experimental evaluation of the second life battery performance. In Section 3, the electrical models are calibrated thanks to the experimental result and their accuracy is evaluated thanks to a mobile charging station and a WLTC profile in Section 4. Finally, conclusions are drawn and an outlook for future studies is given.

2. Second-Life Cell Performance Assessment

This section presents the experiments conducted to assess the performance of a second life battery cell. This performance assessment is necessary to tailor the reuse application to the capabilities of the battery. The data produced for this study are available in a public repository along with a detailed description of the cell and setup characteristics as well as the testing procedures and quality control [32].

2.1. Experimental Setup

In this study, a second life SAMSUNG SDI 94Ah cell with NMC positive electrode was tested at 0, 25 and 40 °C. The main characteristics of the cell are summarized in Table 1. This cell was extracted from a BMW i3 module purchased from the second life battery market. To ensure the representativeness of the study, the 12 cells of the module were tested and one cell with comparable performance to the others was selected.

Table 1. Samsung SDI 94Ah main characteristics. Data from [35].

Characteristics	Values
Format	Prismatic
Nominal capacity [Ah]	94
Positive electrode material	NMC
Negative electrode material	Graphite
Nominal voltage [V]	3.68
Maximal voltage [V]	4.15
Minimal voltage [V]	2.7
Specific energy [Wh/kg]	165
Size L × W × H [mm]	173 × 125 × 45
Weight [kg]	2.06

The experimental setup consisted of a Bitrode battery testing system and two climate chambers (Vötsch VT 3050 and Friocell 707).

Table 2 shows the characterization test protocol at a single temperature and Figure 3 is the voltage profile of the test. Step 1 is a capacity test, consisting of a sequence of three full charge/discharge cycles. Step 2 is an impedance measurement thanks to a sequence of current pulses at different depths of discharge (10, 20, 30, 40, 50, 60, 70, 80 and 90%) and current levels (0.3C, 0.5C, 0.8C, 1C and 1.3C). Step 3 is a pseudo-open circuit voltage measurement thanks to a full discharge/charge at C/20. Finally, step 4 is the validation cycle used to assess the accuracy of the models in mobile charging station usage. The validation profiles and results are described in detail in Sections 3 and 4.

Table 2. Reference characterization test.

Step	Test	Estimated Duration (h)
1	Capacity test	18
2	Impedance test	8
3	Pseudo OCV test	42
4	Mobile charging station cycles	12

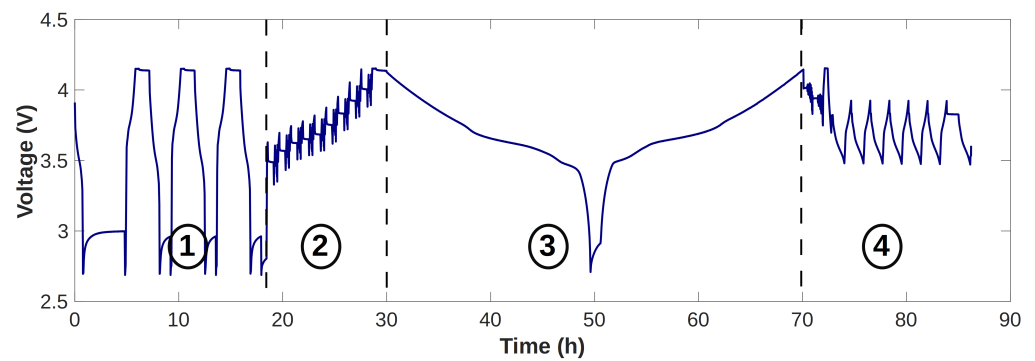


Figure 3. Voltage profile of the test. Step 1 is a capacity test, step 2 is the impedance measurement, step 3 is the low-current measurement and step 4 is the validation cycle.

For the characterization of a cell at 0, 25 and 40 °C, authors estimate that in 273 h (3 times 91 h) the climate chamber consumed 136.5 kWh and the cyclers 94.5 kWh, giving a total consumption of 231 kWh. In France, at the time of the experiment, this electrical consumption generated about 14.7 kg CO₂ eq and cost 53 € [36]. In order to minimize the cost of battery research, the data has been made open access. The authors hope that this data will benefit future research and allow a reduction in the number of experiments conducted.

2.2. Capacity Measurement

The capacity is measured in step 1 of the characterization test shown in Figure 3. The third measurement of discharge capacity in step 1 is taken as the reference and the capacity is calculated according to Equation (A1). Figure 4 shows the influence of temperature on the discharge capacity.

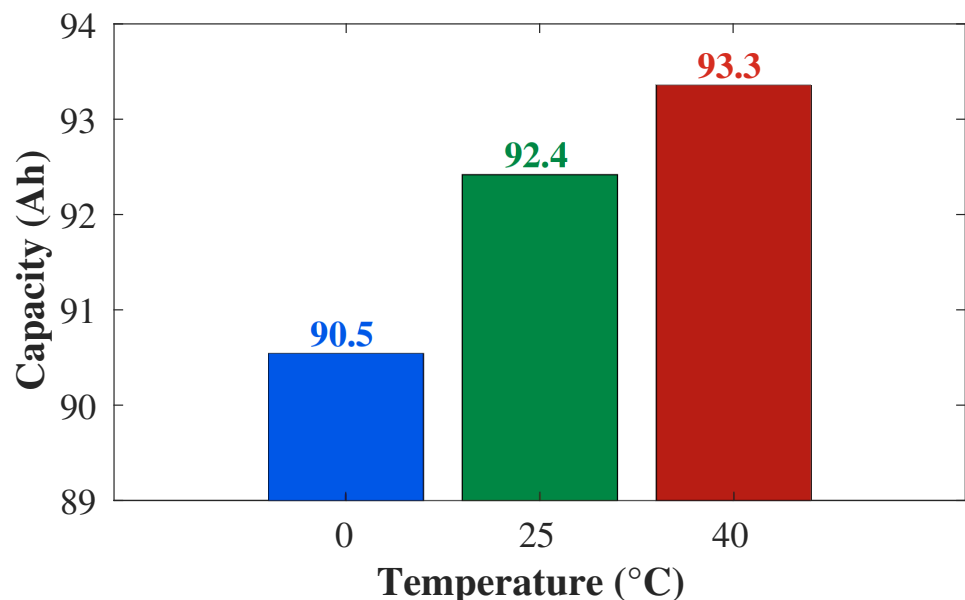


Figure 4. Discharge capacity measured at 0 °C (blue bar), 25 °C (green bar) and 40 °C (red bar).

The capacities listed in the datasheet were measured in discharge with a constant current-constant voltage profile and a 1C current. This method is similar to the one used in this work. A state of health “capacity” can therefore be calculated thanks to Equation (A2). Table 3 compares the capacities measured during step 1 at 0, 25 and 40 °C with the datasheet information.

2.3. Resistance Measurement

Resistance is determined during step 2 of the characterization test presented in Figure 3. Resistance is affected by temperature, sign and intensity of the current and the depth of discharge of the cell. The depth of discharge and resistance are calculated according to Equations (A3) and (A4).

Figure 5 shows the influence of temperature and depth of discharge over the discharge resistance. The measurement is made in discharge with a current rate of $-1C$ and a 5 s resistance is considered.

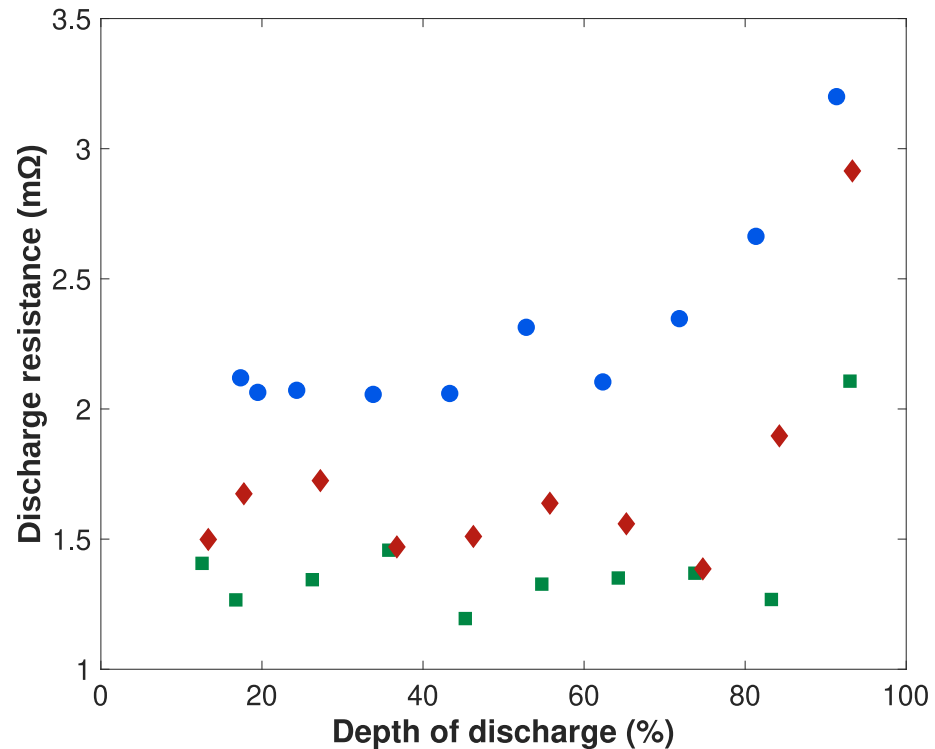


Figure 5. Discharge resistance of a second life cell at 0 (blue points), 25 (green squares) and 40 °C (red diamonds). Measurement is made at $-1C$ and a 5 s resistance is considered.

State of health is an indicator of the evolution of the resistance since the beginning of the battery's life. It can be calculated using Equation (A5). Table 3 compares the resistances measured during step 2 at 0, 25 and 40 °C with the data sheet information.

2.4. Performance Comparison of a Fresh and Second Life Cell

This article evaluates the performance of a high-capacity prismatic cell taken from an electric vehicle. Table 3 compares the capacity and resistance measured on the second life cell with the data provided in the datasheet.

Table 3. Performance comparison between a fresh cell (datasheet) and a second life cell (experiments). “-” means that the state of health could not be calculated.

	Temperature	Fresh Cell	Second Life Cell	State of Health
Capacity (CC-CV, $-1C$)	0 °C	No data	90.5 Ah	-
	25 °C	95.2 Ah	92.4 Ah	97%
	40 °C	95.7 Ah	93.3 Ah	97%
Resistance (5 s, DoD 50%, $-1C$)	0 °C	No data	2.3 mΩ	-
	25 °C	0.75 mΩ	1.3 mΩ	27%
	40 °C	No data	1.6 mΩ	-

The result presented above shows through experimental results that a second life and a fresh cell can perform comparably. This result could be extended to the module level as the tested cell was selected as a representative element of the performance of the 11 other cells in the module. To explain this high level of performance, the authors hypothesize that the tested second life cell came from a crashed vehicle. This study highlights the pertinence of defining the second life battery based on an application change rather than a performance level. Batteries can reach the end of their automotive life with a performance level well above the commonly accepted threshold of 20% capacity loss.

3. Second-Life Cell Modeling

Accurate estimation of a lithium-ion cell's voltage behavior over time is paramount in most applications. In fact, the efficiency of thermal management, energy management, and balancing strategies depends heavily on the accuracy of the estimate [37–41]. In a large number of industrial applications where real-time control is required, electrical models are preferred over electrochemical [42]. Their ability to accurately emulate voltage with limited computational cost makes them suitable for embedded applications. In addition, they can be characterized using non-destructive methods [43–45].

This section presents the equivalent circuit models used in the study and the procedure used to calibrate and validate them. The work presented can be divided into three parts. First, two equivalent circuit models capable of emulating the voltage response of a lithium-ion cell are presented. Then, the parameters of the models at 0, 25 and 40 °C are identified. Finally, the accuracy of each model has been evaluated thanks to two usage profiles: a Worldwide Harmonized Light Vehicles Test Procedures cycle and a profile representative of a real mobile charging station usage. Data processing and modeling have been carried out thanks to two open software: DATTES and VEHLIB.

DATTES is a free and open-source Matlab/Octave set of tools for processing experimental data on energy storage systems [33]. This software is capable of processing data from many different battery cyclers and the most common battery techniques, including capacity and impedance measurements or OCV, ICA and EIS analysis. It allows users to process experimental data using a methodology carefully described in the documentation, or to customize the analysis method according to their needs.

VEHLIB is a free and open-source energy management simulation software for electrified vehicles developed in MATLAB/Simulink [34]. It is based on a block diagram description combined with principles from Bond Graph theory.

3.1. Model Definition

In this article, two equivalent circuit models have been chosen.

The first one is shown in Figure 6 and will be named “CPE model”. It consists of an open circuit voltage (OCV) source in series with two elements: a resistance R_0 which models the ohmic behavior and a Constant Phase Element (CPE) associated with the other dynamic behavior.

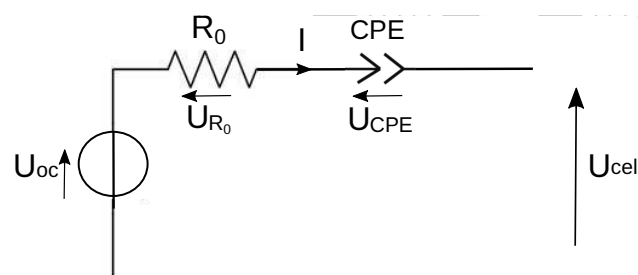


Figure 6. CPE model.

This model emulates the battery voltage response when a current is applied according to Equation (1).

$$U_{cell} = U_{oc} + U_{R0} + U_{CPE} \quad (1)$$

with

- U_{cell} : the voltage response of the cell (V)
- U_{oc} : the open circuit voltage (V)
- U_{R0} : the ohmic drop (V)
- U_{CPE} : the voltage dynamic modeled by the constant phase element (V)

The second model is shown in Figure 7 and will be named “RC model”. It consists of a voltage source OCV in series with resistance R_0 which models the ohmic behavior, a first RC circuit for modeling the charge transfer and double layer processes and a second RC circuit associated with the diffusion behavior. To maximize the model accuracy during relaxation, adding more RC circuits would be necessary [46]. However, this would also dramatically increase the computational time for more advanced simulations using this model. This model emulates the battery voltage response when a current is applied according to Equation (2).

$$U_{cell} = U_{oc} + U_{R0} + U_{R1C1} + U_{R2C2} \quad (2)$$

with

- U_{cell} : the voltage response of the cell (V)
- U_{oc} : the open circuit voltage (V)
- U_{R0} : the ohmic drop (V)
- U_{RiCi} : the voltage dynamic modeled by i-th RC circuit (V)

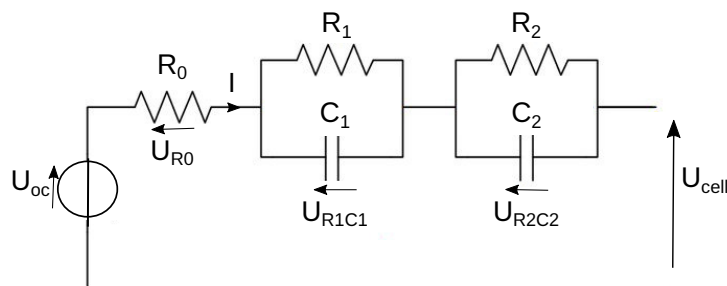


Figure 7. RC model.

For each temperature, the RC and CPE parameters of the models are calibrated in two steps according to the phenomena modeled. The static or thermodynamic behavior is modeled by the open circuit voltage, while the dynamic or polarization behavior is modeled by the parameters $R_0 + CPE$ or $R_0 + R_1C_1 + R_2C_2$.

3.2. Static Behavior Identification

The static behavior of a battery is usually modeled by an open-circuit voltage source whose behavior evolves with the depth of discharge, temperature and state of health of the battery. The influence of aging is not considered in this study.

In this study, the open circuit voltage (OCV) is determined at $C/20$ thanks to step 3 of the test shown in Figure 3. It is calculated by averaging the low rate charge and discharge voltage curves, a technique known as pseudo open circuit voltage. In the datasheet, the open circuit voltage is measured using a galvanostatic intermittent titration technique at $1/3C$. This method is slower but more accurate than pseudo-OCV because it is less subject to current polarization [47]. In this work, pseudo-OCV has been favored for its speed in producing a sufficient number of experimental points to accurately model the dependence of open circuit voltage on the depth of discharge. Figure 8 shows the influence of temperature and depth of discharge on the open circuit voltage.

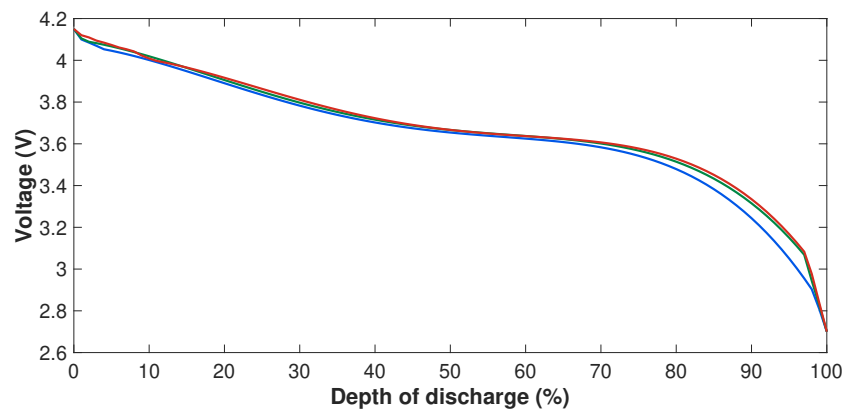


Figure 8. Experimental OCV-DoD relationship curves for second life battery at 0 °C (blue line), 25 °C (green line) and 40 °C (red line).

In order to model the influence of the depth of discharge on the open circuit voltage, 100 experimental points were considered, ranging from 0% to 100% depth of discharge. Linear interpolation is used between two experimental points for intermediate levels of discharge depth. This method was favored as it maximizes accuracy compared to modeling thanks to an equation.

3.3. Dynamic Behavior Identification

The dynamic behavior of a battery is modeled by the impedance parameters of the model. These parameters are influenced by the depth of discharge, temperature and state of health of the battery. The influence of aging is not considered in this study.

The resistance R_0 models the ohmic drop, it is determined first as it is the shortest dynamic phenomenon that will be modeled in this study. The influence of discharge depth and temperature on the resistance was determined experimentally in step 2 of the characterization test shown in Figure 3. To model the influence of discharge depth on R_0 , 10 experimental points were considered from discharge depth 10% to 90% and at a current rate of $-1C$. A logarithmic interpolation is considered between two experimental points for intermediate levels of discharge depth. The influence of the depth of discharge on the 0 s resistance is modeled according to Equation (A6). The result of the resistance interpolation is shown in Figure 9.

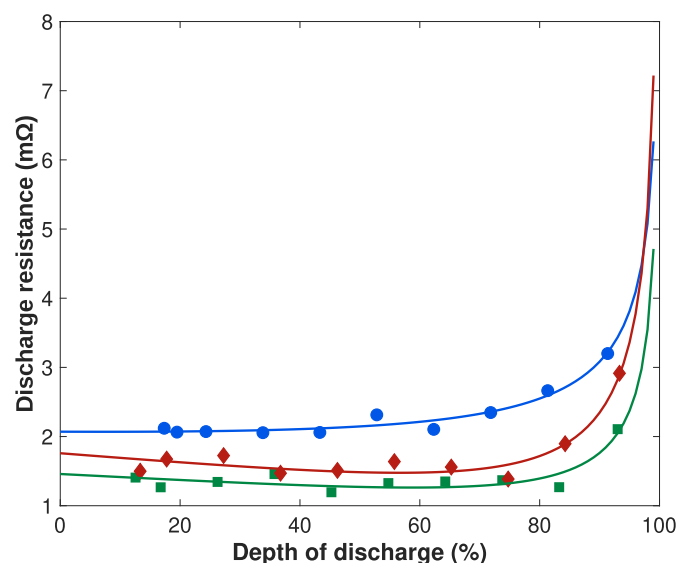


Figure 9. Experimental result and model response (lines) for 0 s discharge resistance versus depth of discharge and temperature 0 (blue), 25 (green) and 40 °C (red).

The parameters R_1, C_1, R_2, C_2, Q and α are intended to emulate the dynamic behavior of a mobile charging station. To model the influence of the depth of discharge on these parameters, 10 experimental points were considered, ranging from a depth of discharge of 10% to 90% and at a current rate of $-1C$. The equations used to model the influence of the depth of discharge on these parameters are presented in Appendix A and the values of models parameters are available in Appendix B.

4. Models Accuracy Assessment

The previous sections presented the identification of model parameters. It consisted in determining the parameters responsible for modeling the different battery dynamics separately thanks to the experimental data collected during the characterization test. In this section, the different parameters are collected to build the RC and CPE models and to validate their accuracy.

4.1. Accuracy on a WLTC Profile

To facilitate comparison with other modeling studies, a popular usage profile was used to validate the model: the worldwide harmonized light vehicles test procedures cycle. Wheel power demand data available for a Golf-GTE PHEV and previously published in [48] were used. In [48], the Golf-GTE PHEV chassis (mass, aerodynamics, rolling resistance, etc.) was used to evaluate the battery demand over the driving cycle. The VEHLIB library was used to perform the simulation [34,49]. Figure 10 shows the Worldwide Harmonized Light Vehicles Test Cycle profile used.

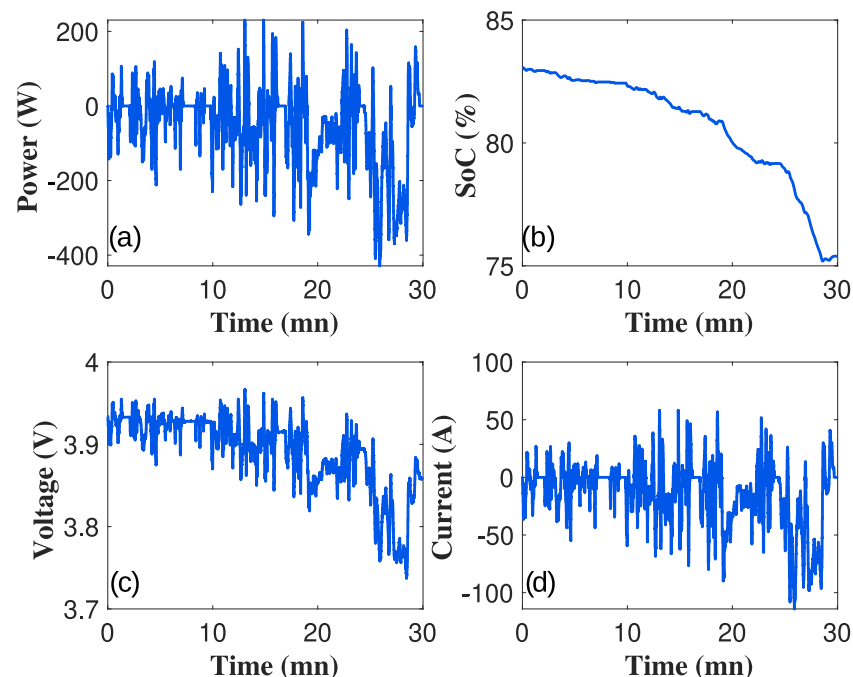


Figure 10. (a) Power, (b) state of charge, (c) voltage and (d) current evolution during a Worldwide Harmonized Light Vehicles Test Cycle profile.

4.1.1. Influence of the Model Choice over Models Accuracy

Figure 11 shows in blue line the second life cell voltage measured at 25 °C and compared to CPE model response in solid line and RC model in dashed line.

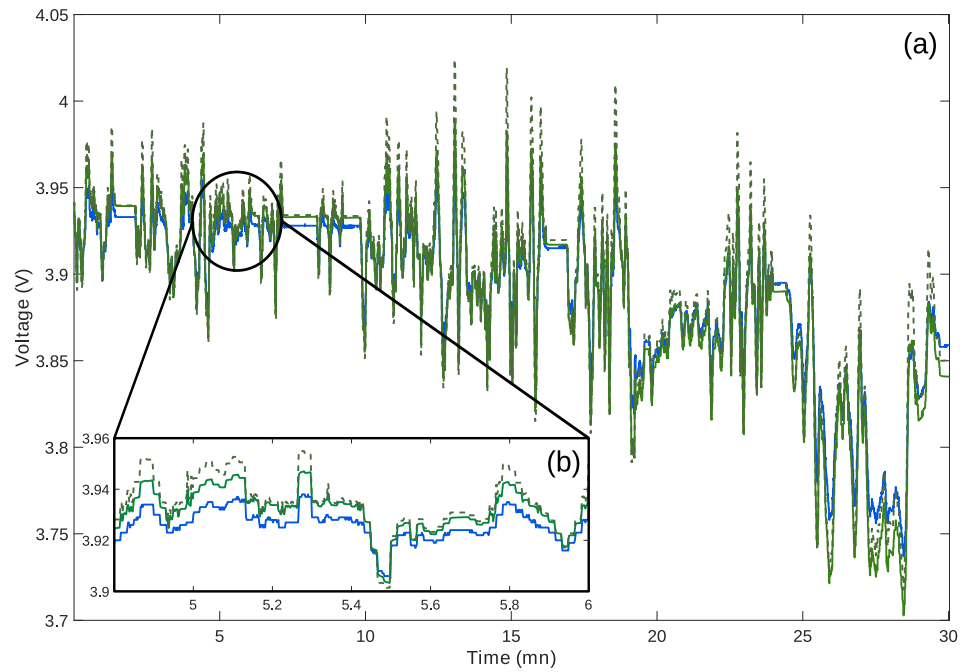


Figure 11. (a) Experimental data (blue line) compared to simulation results for the CPE model (solid line) and the RC model (dashed line) at 25 °C. (b) Zoom around 5 min.

A large part of the error comes from the dynamic behavior, more precisely from the interpolation of the resistance at the intermediate level of the depth of discharge. To improve the accuracy of the models, the parameters responsible for the voltage dynamics, especially at the end of charge and discharge, should be optimized. Efforts could also be made to more accurately account for the relaxation effect.

Figure 12 shows the error distribution functions of the models. For both the CPE model in the solid line and the RC model in the dashed line, the simulation error is less than ± 7 mV, ± 22 mV, and ± 40 mV in 50, 90, and 99% of the profile, respectively.

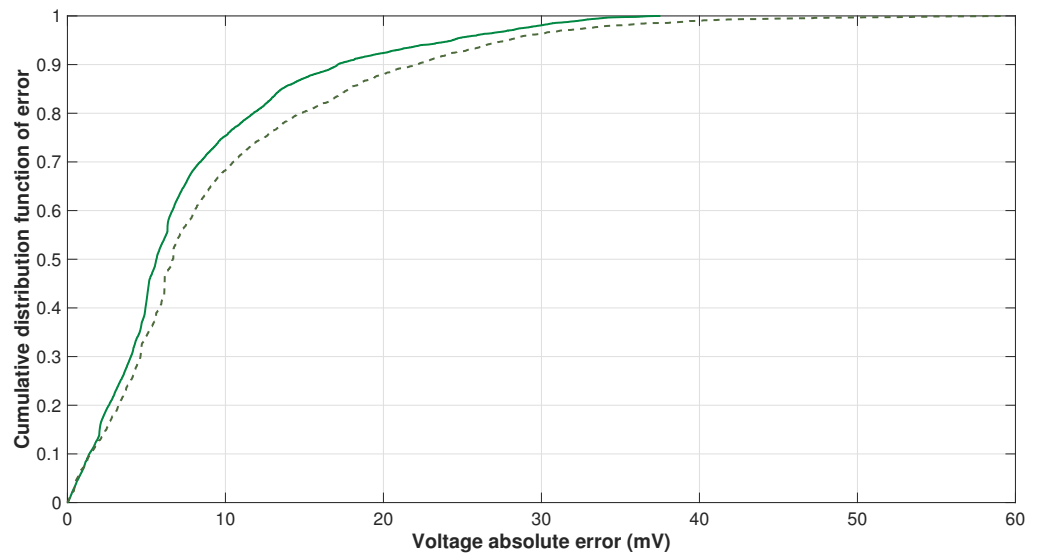


Figure 12. Error distribution functions for the CPE model (solid line) and the RC model (dashed line) emulating a cell voltage response used with a WLTC profile at 25 °C.

4.1.2. Influence of the Temperature over Models Accuracy

In this section, the influence of temperature on model accuracy is assessed thanks to a WLTC profile. Figure 13 presents the influence of temperature on the RC model accuracy. The error distribution function is plotted in blue for 0 °C, green for 25 °C and red for 40 °C.

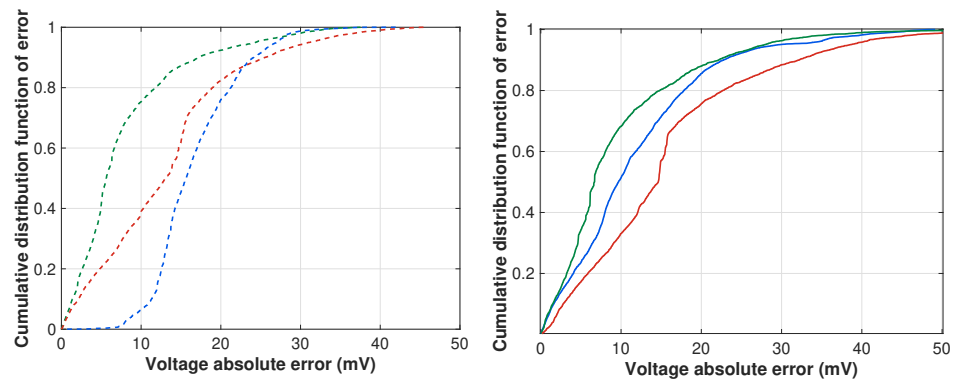


Figure 13. Influence of temperature over RC model ((left), dashed line) and CPE model ((right), solid line) accuracy. Blue lines are at 0 °C, green lines at 25 °C and red lines at 40 °C.

For the RC model, simulation error is lower than ± 16 mV, ± 25 mV and ± 40 mV in, respectively, 50, 90 and 99% of the profile. While for the CPE model, simulation error is lower than ± 15 mV, ± 32 mV and ± 50 mV in, respectively, 50, 90 and 99% of the profile.

4.2. Accuracy on A Mobile Charging Station Profile

A mobile charging station's usage profile inspired by real ones has been used to compare the model's capabilities to emulate the voltage response of the reused batteries. The real usage profiles were provided by the company Mob-Energy. Figure 14 shows the usage profile of the mobile charger with power levels given for a single lithium-ion cell.

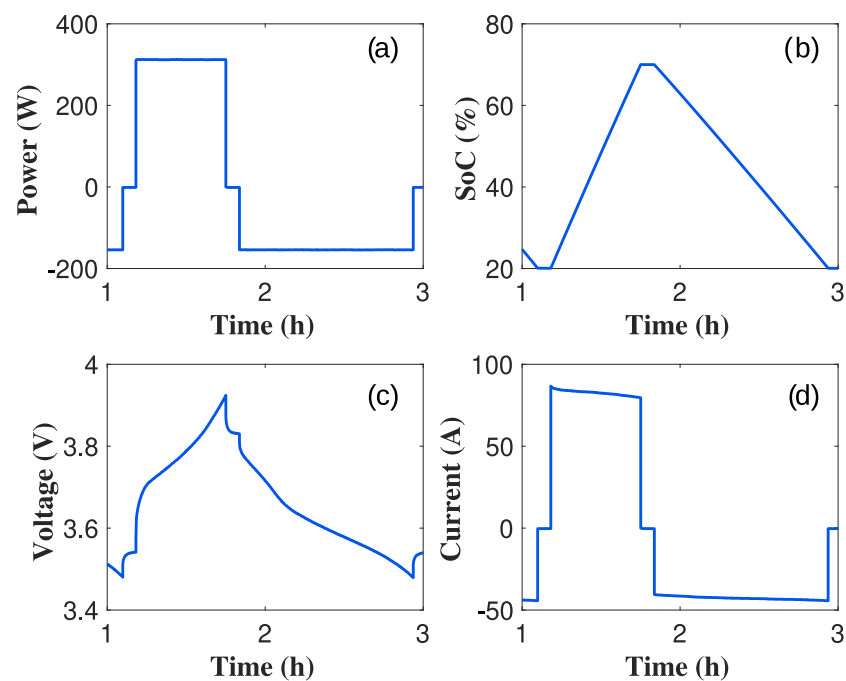


Figure 14. (a) Power, (b) state of charge, (c) voltage and (d) current evolution during a mobile charging station usage profile.

The first step of the profile consists of a high power discharge corresponding to the energy transfer from the charger to the vehicle. In this step, the discharge power reaches -150 W at the cell scale, which corresponds to a 7200 W discharge at the robot scale. Then the robot charger moves to grid charging, which corresponds to the low power discharge (almost 0 W). Finally, the mobile charger is charged from the grid. In this step, the charging power reaches 300 W at the cell scale, which corresponds to a $14,400$ W charge at the robot scale. It can now move on to the next vehicle to charge. This pattern is repeated 12 times in a 24-h period. The voltage, state of charge and current responses of a cell are also shown.

Influence of the Model Choice over Models Accuracy

Figure 15 shows in blue line the second life cell voltage measured with a mobile charger profile at 25 °C. It is compared with the response of the CPE model in the solid line and the RC model in the dashed line. The cumulative distribution function of both models is also shown.

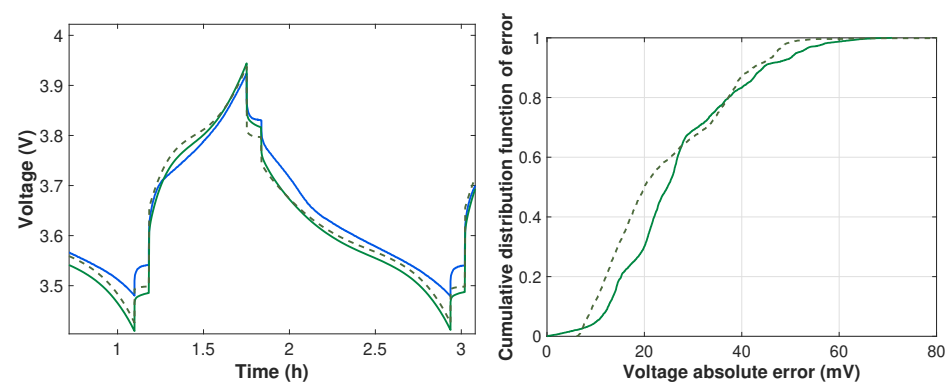


Figure 15. Influence of model choice over accuracy at 25 °C. Left, voltage profile; right error distribution (blue line = measurements, green solid line = CPE model, green dashed line = RC model).

For both the CPE and RC models, the simulation error is less than ± 25 mV, ± 45 mV and ± 61 mV in 50, 90 and 99% of the profile, respectively. The accuracy of the models is lower in this usage profile, which can be explained by the wider range of the depth of discharge. The interpolation of the dynamic parameters in the middle of the depth of discharge is responsible for more than 75% of the model inaccuracy. To improve the accuracy of the models, more experimental data points should be collected and efforts should focus on interpolation techniques.

4.3. Computation Time and Error Assessment

Table 4 shows the accuracy and computation time of the models for different temperatures using a thirty-minute WLTC profile and an eleven-hour mobile charging station profile, respectively. The simulations were run on SIMULINK R2021a with an ode15s solver and a maximum step size of 100 ms. The computer used was a DELL Latitude 5290 laptop with an Intel® Core™ i7-8650U CPU and a clock speed of 1.90 GHz.

CPE and RC models have a comparable absolute average error, but simulation time is significantly in favor of the latter. Both models perform reasonably well, with accuracy levels around 1%, which is in the order of magnitude of models presented in the literature [50–53].

Models are more accurate with the WLTC profile compared to the mobile charging station one. This difference can be explained by the severity of the charger profile. The performance of the models is sufficient to estimate, accurately and with low computational load, the energy stored in the mobile charging station and its efficiency at a given time. These quantities are central for defining optimal pricing, scheduling, and energy management to maximize profits and minimize battery degradation [54–56].

Table 4. Accuracy and computation time for different temperatures using the mobile charging station and WLTC profiles.

			CPE Model	RC Model
WLTC	Accuracy (RMSE)	0 °C	17.5 mV	14.8 mV
		25 °C	10.5 mV	12.9 mV
		40 °C	15.9 mV	19.2 mV
	Computation time	0 °C	11.2 s	3 s
		25 °C	8.7 s	3.1 s
		40 °C	9.9 s	3.3 s
Charger	Accuracy (RMSE)	0 °C	32.6 mV	35.4 mV
		25 °C	29.5 mV	27.2 mV
	Computation time	0 °C	71.9 s	35.6 s
		25 °C	80.8 s	35.1 s

If a better estimation of the energy stored in the charging station at a given time is required, the accuracy of the models could be improved by adding parameters to the models. However, this strategy would certainly increase the computational time, so a trade-off between model accuracy and computational time must be made.

5. Conclusions

This article presents an experimental evaluation of the performance of a second life battery. This experimental work contributes to the existing literature on second life batteries as it is one of the first to evaluate the performance of a high-capacity prismatic cell extracted from an electric vehicle battery pack. The characterization of a cell extracted from an electric vehicle has shown that a second life and a fresh cell can perform comparably. This study highlights the relevance of defining second life batteries based on a change of application rather than a performance threshold between first and second life.

The modeling study conducted has demonstrated the ability of two models to accurately emulate the voltage response of a second life battery. The influence of usage profile and temperature on the accuracy of the models was also evaluated. This study contributes to the development of battery reuse by presenting a new possible application: mobile charging stations. This work is also the first step in the development of pricing, charging schedule, and energy management strategies for battery-powered mobile charging stations.

Finally, this study was conducted with an open-science approach. Characterization data are shared along with a detailed description of the test procedures [32]. Data processing has also been made thanks to two open software: DATTES and VEHLIB [33,34].

Author Contributions: Conceptualization: M.H., E.R.-I. and P.V.; Methodology: M.H., E.R.-I. and P.V.; Software: M.H. and E.R.-I.; Validation: M.H., E.R.-I. and P.V.; Data analysis: M.H.; Writing—original draft preparation: M.H.; Writing—review and editing: E.R.-I. and P.V.; Supervision: E.R.-I. and P.V.; Funding acquisition: E.R.-I. and P.V. All authors have read and agreed to the published version of the manuscript.

Funding: This research was lead as part of the project BAROM funded by Région Auvergne-Rhône-Alpes.

Data Availability Statement: Experimental data are shared on the a public depository at https://data.univ-gustave-eiffel.fr/dataverse/second_life_batteries (accessed on 27 February 2023). Code for data processing is shared at https://dattes.gitlab.io/page/examples/second_life/ (accessed on 27 February 2023).

Acknowledgments: Authors would like to thank Mob-Energy for the collaboration including sharing of a real mobile charging station usage profile. This article supports a project on the use of second life batteries in mobile charging station which would not have been possible without the help of Serge Pelissier, whom we would like to thank.

Conflicts of Interest: The authors declare no conflict of interest.

Abbreviations

The following abbreviations are used in this manuscript:

BOL	Beginning of Life
CC	Constant Current
CPE	Constant Phase Element
CV	Constant Voltage
DoD	Depth of discharge
EIS	Electrochemical Impedance Spectroscopy
ICA	Incremental Capacity Analysis
NMC	Nickel Manganese Cobalt
OCV	Open Circuit Voltage
RMSE	Root Mean Square Error
SoH	Stater of Health
WLTC	Worldwide Harmonized Light Vehicles Test Cycle

Appendix A. Equations

Appendix A.1. Capacity

$$Q(t) = \frac{1}{3600} \int_{t_0}^t i(t) dt \quad (\text{A1})$$

with

- $Q(t)$: the discharge capacity measured (Ah)
- $t - t_0$: the duration of a discharge cycle (s)
- i : the discharge current applied to the cell (A)

Appendix A.2. State of Health Capacity

$$SoH_Q = 100 \times \frac{Q(t)}{Q_{BOL}} \quad (\text{A2})$$

with

- SoH_Q : the state of health “capacity” (%)
- $Q(t)$: the capacity measured at a given time (Ah)
- Q_{BOL} : the capacity measured at the beginning of life (BOL) (Ah)

Appendix A.3. Depth of Discharge

$$DoD = DoD_{t_0} - 100 \times \frac{1}{3600 \times Q_{BOL}} \int_{t_0}^t i(t) dt \quad (\text{A3})$$

with

- DoD : the depth of discharge of the cell (%)
- DoD_{t_0} : the initial cell depth of discharge (%)
- Q_{BOL} : the capacity measured at the beginning of life (BOL) (Ah)
- $i(t)$: the current at a given time (A) (Current is negative in discharge)

Appendix A.4. Pulse Resistance

$$R_{\Delta t}(t) = \frac{\Delta V}{\Delta I} \quad (\text{A4})$$

with

- $R_{\Delta t}(t)$: the resistance measured at a given time (Ω)
- Δt : the time after the pulse beginning (s)

- ΔV : the voltage variation after Δt (V)
- ΔI : the current pulse amplitude (A)

Appendix A.5. State of Health Resistance

$$SoH_R = 100 \times \left(1 - \frac{R(t) - R_{BOL}}{R_{BOL}}\right) \quad (A5)$$

with

- SoH_R : the state of health “resistance” (%)
- $R(t)$: the resistance measured at a given time (m Ω)
- R_{BOL} : the resistance measured at the beginning of life (BOL) (m Ω)

Appendix A.6. Resistance Dependence to Depth of Discharge

$$R(DoD) = r_2 \times \log(DoD)^2 + r_1 \times \log(DoD) + r_0 \quad (A6)$$

with

- $R(DoD)$: the resistance for a given depth of discharge (Ω)
- r_i : the polynomial coefficient of the model (Ω)

Appendix A.7. C1 Dependence to Depth of Discharge

$$C1(DoD) = c_{1,3} \times (DoD)^3 + c_{1,2} \times (DoD)^2 + c_{1,1} \times (DoD) + c_{1,0} \quad (A7)$$

with

- $C1(DoD)$: the resistance for a given depth of discharge (F)
- c_i : the polynomial coefficient of the model (F)

Appendix A.8. RC Impedance

$$Z_{RC}(jw) = \frac{1}{1 + RCjw} \quad (A8)$$

with

- $Z_{RC}(jw)$: the RC impedance (Ω)
- R : the resistance (Ω)
- C : the capacitor (F)

Appendix A.9. R1C1 Pulse Response Voltage

$$U_{R1C1} = I_{cell} \times \exp\left(\frac{-t}{\tau_1}\right) \quad (A9)$$

with

- U_{R1C1} : the voltage polarization caused by R_1C_1 (V)
- τ_1 : the polarization time constant of the fastest dynamic phenomena (s)

Appendix A.10. R2C2 Pulse Response Voltage

$$U_{R2C2} = I_{cell} \times \exp\left(\frac{-t}{\tau_2}\right) \quad (A10)$$

with

- U_{R2C2} : the voltage polarization caused by R_2C_2 (V)
- τ_2 : the polarization time constant of the fastest dynamic phenomena (s)

Appendix A.11. CPE Impedance

$$Z_{CPE}(j\omega) = \frac{1}{Q(j\omega)^\alpha} \quad (A11)$$

with

- $Z_{CPE}(j\omega)$: the CPE impedance (Ω)
- $Q(DoD)$: the main CPE element for a given depth of discharge ($\Omega^{-1}s^\alpha$)
- α : the depression factor of the CPE (-)

Appendix A.12. CPE Voltage

$$U_{CPE}(t) = I_{cell} \times \frac{(t - t_1)^\alpha - (t - t_2)^\alpha}{Q \times \Gamma(\alpha + 1)} \quad (A12)$$

with

- U_{CPE} : the voltage polarization caused by the CPE element (V)
- t_1 : the time at the beginning of the pulse (s)
- t_2 : the time at the end of the pulse (s)
- α : the depression factor of the CPE (-)
- Q : the main CPE element ($\Omega^{-1}s^\alpha$)
- Γ : the Gamma function

Appendix A.13. Gamma Function

$$\Gamma(\alpha) = \int_0^\infty t^{\alpha-1} \times 10^{-t} dt \quad (A13)$$

with

- Γ : the Gamma function
- t : the time (s)
- α : the depression factor of the CPE (-)

Appendix B. Models Parameters

Table A1. OCV models parameters for DoD from 1% to 9%.

DoD	1	2	3	4	5	6	7	8	9
OCV	4.150	4.099	4.080	4.069	4.053	4.046	4.038	4.029	4.021
	4.150	4.105	4.089	4.082	4.075	4.067	4.058	4.049	4.039
	4.150	4.120	4.109	4.094	4.084	4.073	4.061	4.053	4.042

Table A2. OCV models parameters for DoD from 10% to 19%.

DoD	10	11	12	13	14	15	16	17	18	19
OCV	4.011	4.001	3.991	3.981	3.969	3.959	3.948	3.936	3.925	3.913
	4.029	4.019	4.008	3.997	3.986	3.975	3.964	3.952	3.940	3.929
	4.023	4.009	3.997	3.990	3.982	3.974	3.965	3.956	3.947	3.937

Table A3. OCV models parameters for DoD from 20% to 29%.

DoD	20	21	22	23	24	25	26	27	28	29
OCV	3.902	3.890	3.879	3.867	3.856	3.845	3.834	3.823	3.813	3.803
	3.917	3.905	3.894	3.882	3.871	3.859	3.849	3.838	3.827	3.817
	3.927	3.916	3.906	3.895	3.885	3.874	3.863	3.853	3.842	3.831

Table A4. OCV models parameters for DoD from 30% to 39%.

DoD	30	31	32	33	34	35	36	37	38	39
OCV	3.792	3.783	3.773	3.764	3.755	3.745	3.738	3.730	3.723	3.716
	3.807	3.797	3.788	3.778	3.769	3.761	3.752	3.744	3.737	3.729
	3.821	3.811	3.801	3.791	3.781	3.772	3.763	3.754	3.746	3.738

Table A5. OCV models parameters for DoD from 40% to 49%.

DoD	40	41	42	43	44	45	46	47	48	49
OCV	3.709	3.702	3.696	3.690	3.685	3.679	3.674	3.669	3.665	3.661
	3.722	3.716	3.709	3.703	3.698	3.692	3.687	3.682	3.678	3.674
	3.730	3.723	3.716	3.709	3.702	3.696	3.690	3.685	3.680	3.675

Table A6. OCV models parameters for DoD from 50% to 59%.

DoD	50	51	52	53	54	55	56	57	58	59
OCV	3.658	3.654	3.651	3.647	3.644	3.641	3.639	3.636	3.633	3.630
	3.669	3.666	3.663	3.659	3.656	3.653	3.651	3.648	3.645	3.643
	3.671	3.667	3.663	3.659	3.656	3.653	3.649	3.647	3.644	3.642

Table A7. OCV models parameters for DoD from 60% to 69%.

DoD	60	61	62	63	64	65	66	67	68	69
OCV	3.628	3.625	3.622	3.619	3.616	3.612	3.608	3.604	3.599	3.595
	3.640	3.637	3.635	3.632	3.629	3.626	3.623	3.619	3.615	3.611
	3.639	3.637	3.634	3.632	3.629	3.627	3.624	3.621	3.618	3.615

Table A8. OCV models parameters for DoD from 70% to 79%.

DoD	70	71	72	73	74	75	76	77	78	79
OCV	3.589	3.583	3.577	3.569	3.561	3.552	3.543	3.532	3.520	3.508
	3.606	3.601	3.596	3.589	3.583	3.576	3.568	3.559	3.549	3.538
	3.611	3.607	3.602	3.597	3.591	3.585	3.577	3.569	3.561	3.551

Table A9. OCV models parameters for DoD from 80% to 89%.

DoD	80	81	82	83	84	85	86	87	88	89
OCV	3.494	3.479	3.463	3.445	3.426	3.405	3.383	3.359	3.333	3.305
	3.527	3.514	3.500	3.486	3.469	3.452	3.433	3.413	3.390	3.367
	3.540	3.529	3.516	3.502	3.486	3.469	3.451	3.431	3.410	3.387

Table A10. OCV models parameters for DoD from 90% to 100%.

DoD	90	91	92	93	94	95	96	97	98	99	100
OCV	3.275	3.244	3.209	3.173	3.135	3.094	3.050	3.004	2.955	2.903	2.700
	3.342	3.315	3.286	3.255	3.222	3.187	3.150	3.110	3.068	2.944	2.700
	3.362	3.335	3.306	3.275	3.241	3.205	3.167	3.127	3.083	2.977	2.700

Table A11. R0 models parameters in discharge.

R0 Discharge			
Temperature	$r_{0,2,dch}$	$r_{0,1,dch}$	$r_{0,0,dch}$
0 °C	5.746×10^{-4}	-4.720×10^{-3}	1.157×10^{-2}
25 °C	1.259×10^{-4}	8.614×10^{-4}	5.356×10^{-3}
40 °C	-1.501×10^{-4}	9.962×10^{-4}	-9.188×10^{-5}

Table A12. R0 models parameters in charge.

R0 Charge			
Temperature	$r_{0,2,ch}$	$r_{0,1,ch}$	$r_{0,0,ch}$
0 °C	6.953×10^{-4}	-5.542×10^{-3}	1.311×10^{-2}
25 °C	-5.455×10^{-5}	2.307×10^{-2}	5.995×10^{-3}
40 °C	2.273×10^{-4}	-1.776×10^{-3}	5.070×10^{-3}

Table A13. R1 models parameters.

R1			
Temperature	$r_{1,2}$	$r_{1,1}$	$r_{1,0}$
0 °C	2.037×10^{-4}	-1.697×10^{-3}	4.208×10^{-3}
25 °C	5.111×10^{-5}	-5.698×10^{-4}	1.847×10^{-4}
40 °C	6.204×10^{-5}	-4.265×10^{-4}	1.405×10^{-3}

Table A14. R2 models parameters.

R2			
Temperature	$r_{2,2}$	$r_{2,1}$	$r_{2,0}$
0 °C	5.399×10^{-6}	-2.517×10^{-5}	2.366×10^{-5}
25 °C	2.813×10^{-6}	-1.355×10^{-5}	1.555×10^{-5}
40 °C	5.994×10^{-7}	-3.216×10^{-6}	6.739×10^{-6}

Table A15. C1 and C2 models parameters.

		C1			C2
Temperature	$c_{1,3}$	$c_{1,2}$	$c_{1,1}$	$c_{1,0}$	C2
0 °C	-3.094	547	-3.119×10^4	6.601×10^5	58,422
25 °C	-2.517	380.3	-1.765×10^4	4.053×10^5	62,841
40 °C	-1.610	178.7	-3902	1.703×10^5	95,467

Table A16. Q and α models parameters.

Temperature	Q	α
0 °C	3873	0.1
25 °C	4852	0.1
40 °C	5812	0.1

References

- IPCC. *Climate Change 2022: Mitigation of Climate Change*; Contribution of Working Group III to the Sixth Assessment Report of the Intergovernmental Panel on Climate Change; IPCC: Geneva, Switzerland, 2022.
- IEA. *Global EV Outlook 2021*; IEA: Paris, France, 2021.
- IEA. *Global Supply Chains of EV Batteries*; IEA: Paris, France, 2022.
- Larcher, D.; Tarascon, J.M. Towards greener and more sustainable batteries for electrical energy storage. *Nat. Chem.* **2015**, *7*, 19–29. [[CrossRef](#)] [[PubMed](#)]
- European Union. Directive 2008/98/EC of the European Parliament and the Council of 19 November 2008 on Waste and Repealing Certain Directives. *Off. J. Eur. Union* **2008**, L 312/3. Available online: <http://data.europa.eu/eli/dir/2008/98/oj> (accessed on 26 February 2023).
- Ellingsen, L.A.W.; Singh, B.; Strømman, A.H. The size and range effect: Lifecycle greenhouse gas emissions of electric vehicles. *Environ. Res. Lett.* **2016**, *11*, 054010. [[CrossRef](#)]
- Redondo-Iglesias, E.; Vinot, E.; Venet, P.; Pelissier, S. Electric vehicle range and battery lifetime: A trade-off. In Proceedings of the Electric Vehicle Symposium (EVS32), Lyon, France, 21–22 May 2019.
- Kong, P.Y. Autonomous Robot-Like Mobile Chargers for Electric Vehicles at Public Parking Facilities. *IEEE Trans. Smart Grid* **2019**, *10*, 5952–5963. [[CrossRef](#)]
- Hassini, M.; Redondo-Iglesias, E.; Venet, P.; Gillet, S.; Zitouni, Y. Second-life batteries in a Mobile Charging Station: Model Based Performance Assessment. In Proceedings of the 35th International Electric Vehicle Symposium and Exhibition (EVS35), Oslo, Norway, 11–15 June 2022.

10. Mob-Energy. Mob-Energy. Available online: <https://www.mob-energy.com/en/home> (accessed on 27 March 2023).
11. Volkswagen. The Mobile Charging Robot—Presenting a Vision. Available online: <https://www.volkswagen-newsroom.com/> (accessed on 27 March 2023).
12. Afshar, S.; Macedo, P.; Mohamed, F.; Disfani, V. Mobile charging stations for electric vehicles—A review. *Renew. Sustain. Energy Rev.* **2021**, *152*. [[CrossRef](#)]
13. European Commission. *Sustainable Batteries Regulation*; European Commission: Brussel, Belgium, 2020.
14. Braco, E.; San Martín, I.; Berrueta, A.; Sanchis, P.; Ursúa, A. Experimental assessment of cycling ageing of lithium-ion second life batteries from electric vehicles. *J. Energy Storage* **2020**, *32*, 101695. [[CrossRef](#)]
15. Abdel-Monem, M.; Hegazy, O.; Omar, N.; Trad, K.; De Breucker, S.; Van Den Bossche, P.; Van Mierlo, J. Design and analysis of generic energy management strategy for controlling second life battery systems in stationary applications. *Energies* **2016**, *9*, 889. [[CrossRef](#)]
16. Seger, P.V.; Rigo-Mariani, R.; Thivel, P.X.; Riu, D. A storage degradation model of Li-ion batteries to integrate ageing effects in the optimal management and design of an isolated microgrid. *Appl. Energy* **2023**, *333*. [[CrossRef](#)]
17. Etxandi-Santolaya, M.; Canals Casals, L.; Amante García, B.; Corchero, C. Circular Economy-Based Alternatives beyond Second-Life Applications: Maximizing the Electric Vehicle Battery First Life. *World Electr. Veh. J.* **2023**, *14*, 66. [[CrossRef](#)]
18. Hossain, E.; Murtaugh, D.; Mody, J.; Faruque, H.M.R.; Sunny, M.S.H.; Mohammad, N. A comprehensive review on second life batteries: Current state, manufacturing considerations, applications, impacts, barriers & potential solutions, business strategies, and policies. *IEEE Access* **2019**, *7*, 73215–73252. [[CrossRef](#)]
19. Haram, M.H.S.M.; Lee, J.W.; Ramasamy, G.; Ngu, E.E.; Thiagarajah, S.P.; Lee, Y.H. Feasibility of utilising second life EV batteries: Applications, lifespan, economics, environmental impact, assessment, and challenges. *Alex. Eng. J.* **2021**, *60*, 4517–4536. [[CrossRef](#)]
20. Montes, T.; Etxandi-Santolaya, M.; Eichman, J.; Ferreira, V.J.; Trilla, L.; Corchero, C. Procedure for Assessing the Suitability of Battery Second Life Applications after EV First Life. *Batteries* **2022**, *8*, 122. [[CrossRef](#)]
21. Martínez-Laserna, E.; Sarasketa-Zabala, E.; Sarria, I.V.; Stroe, D.I.; Swierczynski, M.; Warnecke, A.; Timmermans, J.-M.; Goutam, S.; Omar, N.; Rodríguez, P. Technical Viability of Battery Second Life: A Study From the Ageing Perspective. *IEEE Trans. Ind. Appl.* **2018**, *54*, 2703–2713. [[CrossRef](#)]
22. Debnath, U.K.; Ahmad, I.; Habibi, D. Quantifying economic benefits of second life batteries of gridable vehicles in the smart grid. *Int. J. Electr. Power Energy Syst.* **2014**, *63*, 577–587. [[CrossRef](#)]
23. Attia, P.; Bills, A.; Planella, F.B.; Dechent, P.; Dos Reis, G.; Dubarry, M.; Gasper, P.; Gilchrist, R.; Greenbank, S.; Howey, D.; et al. “Knees” in lithium-ion battery aging trajectories. *J. Electrochem. Soc.* **2022**, *169*, 060517. [[CrossRef](#)]
24. Dos Reis, G.; Strange, C.; Yadav, M.; Li, S. Lithium-ion battery data and where to find it. *Energy AI* **2021**, *5*, 100081. [[CrossRef](#)]
25. Coron, E.; Geniès, S.; Cugnet, M.; Thivel, P.X. High-Energy Li-Ion Cells: Impact of Electrode Ageing on Second Life Viability. *J. Electrochem. Soc.* **2021**, *168*, 100539. [[CrossRef](#)]
26. Seger, P.V.; Thivel, P.X.; Riu, D. A second life Li-ion battery ageing model with uncertainties: From cell to pack analysis. *J. Power Sources* **2022**, *541*, 231663. [[CrossRef](#)]
27. Michelini, E.; Höschle, P.; Ratz, F.; Stadlbauer, M.; Rom, W.; Ellersdorfer, C.; Moser, J. Potential and Most Promising Second-Life Applications for Automotive Lithium-Ion Batteries Considering Technical, Economic and Legal Aspects. *Energies* **2023**, *16*, 2830. [[CrossRef](#)]
28. Rallo, H.; Casals, L.C.; De La Torre, D.; Reinhardt, R.; Marchante, C.; Amante, B. Lithium-ion battery 2nd life used as a stationary energy storage system: Ageing and economic analysis in two real cases. *J. Clean. Prod.* **2020**, *272*, 122584. [[CrossRef](#)]
29. Quinard, H.; Redondo-Iglesias, E.; Pelissier, S.; Venet, P. Fast Electrical Characterizations of High-Energy Second Life Lithium-Ion Batteries for Embedded and Stationary Applications. *Batteries* **2019**, *5*, 33. [[CrossRef](#)]
30. Braco, E.; San Martín, I.; Berrueta, A.; Sanchis, P.; Ursúa, A. Experimental assessment of first-and second life electric vehicle batteries: Performance, capacity dispersion, and aging. *IEEE Trans. Ind. Appl.* **2021**, *57*, 4107–4117. [[CrossRef](#)]
31. Albuquerque, L.; Lacressonnière, F.; Roboam, X.; Forgez, C. Incremental Capacity Analysis as a diagnostic method applied to second life Li-ion batteries. In Proceedings of the Electrimacs 2022, Nancy, France, 16–19 May 2022.
32. Hassini, M. Dataset Second-life battery Characterization Test. Available online: https://data.univ-gustave-eiffel.fr/dataverse/second_life_batteries (accessed on 27 March 2023).
33. Redondo-Iglesias, E.; Hassini, M. Data Analysis Tools for Tests on Energy Storage. Available online: <https://dattes.gitlab.io> (accessed on 27 March 2023).
34. Jeanneret, B. VEHLIB. Available online: <https://gitlab.univ-eiffel.fr/eco7/vehlib> (accessed on 27 March 2023).
35. PushEV. Samsung SDI 94Ah battery cell full specifications. Available online: <https://pushevs.com/2018/04/05/samsung-sdi-94-ah-battery-cell-full-specifications/> (accessed on 31 March 2023).
36. RTE, France’s Transmission System Operator. eCO2mix—All of France’s Electricity Data in Real Time. Available online: <https://www.rte-france.com/en/eco2mix/> (accessed on 27 March 2023).
37. Damay, N.; Forgez, C.; Bichat, M.P.; Friedrich, G. Thermal modeling of large prismatic LiFePO₄/graphite battery. Coupled thermal and heat generation models for characterization and simulation. *J. Power Sources* **2015**, *283*, 37–45. [[CrossRef](#)]
38. Lievre, A.; Sari, A.; Venet, P.; Hijazi, A.; Ouattara-Brigaudet, M.; Pelissier, S. Practical online estimation of lithium-ion battery apparent series resistance for mild hybrid vehicles. *IEEE Trans. Veh. Technol.* **2015**, *65*, 4505–4511. [[CrossRef](#)]

39. Shili, S.; Hijazi, A.; Sari, A.; Lin-Shi, X.; Venet, P. Balancing Circuit New Control for Supercapacitor Storage System Lifetime Maximization. *IEEE Trans. Power Electron.* **2017**, *32*, 4939–4948. [[CrossRef](#)]
40. Ndiaye, A.; Locment, F.; De Bernardinis, A.; Sechilariu, M.; Redondo-Iglesias, E. A Techno-Economic Analysis of Energy Storage Components of Microgrids for Improving Energy Management Strategies. *Energies* **2022**, *15*, 1556. [[CrossRef](#)]
41. Parthasarathy, C.; Laaksonen, H.; Redondo-Iglesias, E.; Pelissier, S. Aging aware adaptive control of Li-ion battery energy storage system for flexibility services provision. *J. Energy Storage* **2023**, *57*, 106268. [[CrossRef](#)]
42. Seaman, A.; Dao, T.S.; McPhee, J. A survey of mathematics-based equivalent-circuit and electrochemical battery models for hybrid and electric vehicle simulation. *J. Power Sources* **2014**, *256*, 410–423. [[CrossRef](#)]
43. Tran, M.K.; DaCosta, A.; Mevawalla, A.; Panchal, S.; Fowler, M. Comparative study of equivalent circuit models performance in four common lithium-ion batteries: LFP, NMC, LMO, NCA. *Batteries* **2021**, *7*, 51. [[CrossRef](#)]
44. Nikolian, A.; Jaguemont, J.; De Hoog, J.; Goutam, S.; Omar, N.; Van Den Bossche, P.; Van Mierlo, J. Complete cell-level lithium-ion electrical ECM model for different chemistries (NMC, LFP, LTO) and temperatures (−5 °C to 45 °C). Optimized modelling techniques. *Int. J. Electr. Power Energy Syst.* **2018**, *98*, 133–146. [[CrossRef](#)]
45. Sun, L.; Li, G.; You, F. Combined internal resistance and state-of-charge estimation of lithium-ion battery based on extended state observer. *Renew. Sustain. Energy Rev.* **2020**, *131*, 109994. [[CrossRef](#)]
46. Li, A.; Pelissier, S.; Venet, P.; Gyan, P. Fast Characterization Method for Modeling Battery Relaxation Voltage. *Batteries* **2016**, *2*, 7. [[CrossRef](#)]
47. Dubarry, M.; Baure, G. Perspective on Commercial Li-ion Battery Testing, Best Practices for Simple and Effective Protocols. *Electronics* **2020**, *9*, 152. [[CrossRef](#)]
48. Patil, T.D.; Vinot, E.; Ehrenberger, S.; Trigui, R.; Redondo-Iglesias, E. Sensitivity Analysis of Battery Aging for Model-Based PHEV Use Scenarios. *Energies* **2023**, *16*, 1749. [[CrossRef](#)]
49. Jeanneret, B.; Trigui, R.; Badin, F.; Harel, F.; Damemme, F. New Hybrid concept simulation tools, evaluation on the Toyota Prius car. In Proceedings of the 16th International Electric Vehicle Symposium, Beijing, China, 12–16 October 1999.
50. Baghdadi, I.; Briat, O.; Eddahech, A.; Vinassa, J.M.; Gyan, P. Electro-thermal model of lithium-ion batteries for electrified vehicles applications. In Proceedings of the 2015 IEEE 24th International Symposium on Industrial Electronics (ISIE, Buzios, Brazil, 3–5 April 2015; pp. 1248–1252. [[CrossRef](#)]
51. Seger, P.V.; Coron, E.; Thivel, P.X.; Riu, D.; Cugnet, M.; Genies, S. Open data model parameterization of a second life Li-ion battery. *J. Energy Storage* **2021**, *47*, 103546. [[CrossRef](#)]
52. Quelin, A.; Damay, N. Coupling electrical parameters of a battery equivalent circuit model to electrodes dimensions. *J. Power Sources* **2023**, *561*, 232690. [[CrossRef](#)]
53. Juston, M.; Damay, N.; Forgez, C. Extracting the diffusion resistance and dynamic of a battery using pulse tests. *J. Energy Storage* **2023**, *57*, 106199. [[CrossRef](#)]
54. Afshar, S.; Disfani, V. Optimal Scheduling of Electric Vehicles in the Presence of Mobile Charging Stations. In Proceedings of the IEEE Power & Energy Society General Meeting (PESGM), Denver, CO, USA, 17–21 July 2022. [[CrossRef](#)]
55. Saboori, H.; Jadid, S.; Savaghebi, M. Optimal Management of Mobile Battery Energy Storage as a Self-Driving, Self-Powered and Movable Charging Station to Promote Electric Vehicle Adoption. *Energies* **2021**, *14*, 736. [[CrossRef](#)]
56. Houbbadi, A.; Trigui, R.; Pelissier, S.; Redondo-Iglesias, E.; Bouton, T. Optimal scheduling to manage an electric bus fleet overnight charging. *Energies* **2019**, *12*, 2727. [[CrossRef](#)]

Disclaimer/Publisher’s Note: The statements, opinions and data contained in all publications are solely those of the individual author(s) and contributor(s) and not of MDPI and/or the editor(s). MDPI and/or the editor(s) disclaim responsibility for any injury to people or property resulting from any ideas, methods, instructions or products referred to in the content.